Negative differential resistance induced by Mn substitution at $SrRuO_3$/Nb:$SrTiO_3$ Schottky interfaces

Yasuyuki Hikita,[1,*] Lena Fitting Kourkoutis,[2] Tomofumi Susaki,[1,†] David A. Muller,[2] Hidenori Takagi,[1] and Harold Y. Hwang[1,3]

[1]*Department of Advanced Materials Science, University of Tokyo, Kashiwa, Chiba 277-8561, Japan*

[2]*School of Applied and Engineering Physics, Cornell University, Ithaca, New York 14853, USA*

[3]*Japan Science and Technology Agency, Kawaguchi, Saitama 332-0012, Japan*

(Received 19 March 2008; revised manuscript received 30 April 2008; published 29 May 2008)

We observed a strong modulation in the current-voltage characteristics of $SrRuO_3$/Nb:$SrTiO_3$ Schottky junctions by Mn substitution in $SrRuO_3$, which induces a metal-insulator transition in the bulk. The temperature dependence of the junction ideality factor indicates an increased spatial inhomogeneity of the interface potential with substitution. Furthermore, negative differential resistance was observed at low temperatures, indicating the formation of a resonant state by Mn substitution. By spatially varying the position of the Mn dopants across the interface with single unit cell control, we can isolate the origin of this resonant state to the interface $SrRuO_3$ layer. These results demonstrate a conceptually different approach to controlling the interface states by utilizing the highly sensitive response of conducting perovskites to impurities.

DOI: 10.1103/PhysRevB.77.205330 PACS number(s): 73.40.Sx, 73.40.Gk

I. INTRODUCTION

Schottky junctions using perovskite oxides are systems in which several interesting device properties have been reported including resistance switching,[1] magnetic field sensitive diode,[2] and as a prototypical structure for enhanced photocarrier doping.[3] One of the important concepts in Schottky junctions is the formation of interface states that strongly influence barrier formation and, in many cases, are responsible for nonideal device performance.[4] In elemental metal/conventional semiconductor junctions, the interface states are formed as consequences of intrinsic surface reconstructions, impurities, or defects on the semiconductor surfaces, or alloying by a metal-semiconductor reaction. In many cases, the barrier formation processes are predominantly driven by the properties of the *semiconductor* and are usually less dependent on the properties of the metal with some exceptions such as in the presence of metal-induced-gap states.[5] This is due to the large difference in the bonding character of the constituents, namely spatially oriented covalent bonds in semiconductors and spatially uniform metallic bonds in the metal, which can easily result in amorphous or polycrystalline interfaces.

In contrast, the chemical and structural similarities between metallic and semiconducting perovskites enable the epitaxial growth of oxide heterojunctions. Furthermore, the electrical conductivity in metallic perovskites is often achieved by the delicate energy balance between competing ground states, as seen in high-T_c cuprates or colossal magnetoresistive manganites.[6] Upon doping, many perovskite metals transition through a carrier localized state long before completely becoming an insulator with a well-defined gap in the density of states. When interfaces are formed using such disordered metals, a new type of interface state formation can be anticipated, giving us an additional degree of freedom to manipulate the interface electronic structure from the *metal* side.

To explore these ideas, we have investigated controlled impurity substitution in the $SrRuO_3$/Nb:$SrTiO_3$ junctions. This is an ideal system to study because the interface is free from polar discontinuity, which can be a significant source of interface states,[7] and its barrier formation is not dominated by the interface states, as evidenced by the good agreement between the experimentally determined Schottky barrier height[8,9] and the Schottky–Mott relation. Additionally, Nb:$SrTiO_3$ has been the most thoroughly investigated perovskite semiconductor in junction structures such as the Schottky barrier height characterization,[8] and the studies of nonlinear dielectric constant and its effect on band bending.[10,11] $SrRuO_3$, in the absence of chemical substitution, is a representative conducting perovskite with a ferromagnetic transition temperature T_C=160 K. It exhibits several unusual transport properties such as the absence of resistivity saturation up to 1000 K.[12] The strong divergence of dR/dT as $T \rightarrow T_C^+$ and the weak divergence when $T \rightarrow T_C^-$ raises questions of the applicability of the standard Boltzmann transport picture, leading to the assignment of $SrRuO_3$ as a "bad metal."[13] As can be expected from the unusual behavior in its pure form, $SrRuO_3$ is highly sensitive to the disorder induced by chemical doping such as Ca,[14] Zn, Ni, Co,[15] Fe,[16] or Mn (Refs. 15, 17, and 18) doping, all of which induce metal-insulator transitions. In the case of doping with a 3*d* transition metal ion at the Ru site, the Ru-O bonding network is reduced and carrier localization occurs because of the localized nature of the 3*d* orbitals.

Here, we study the effects of using a strongly correlated metal at the junction interface by examining the temperature-dependent *I-V* characteristics of the Mn-doped $SrRuO_3$/Nb:$SrTiO_3$ Schottky junctions. From the high temperature slope in the semilogarithmic plot of the *I-V* characteristics, the spatial distribution of the barrier height was increased by the Mn substitution. At low temperatures, we observed negative differential resistance even for a single layer of the Mn substituted $SrRuO_3$ metal at the interface. These results indicate that the high sensitivity of strongly correlated metals to impurities can give rise to characteristic interface state formation from imperfectly screened impurity ions.

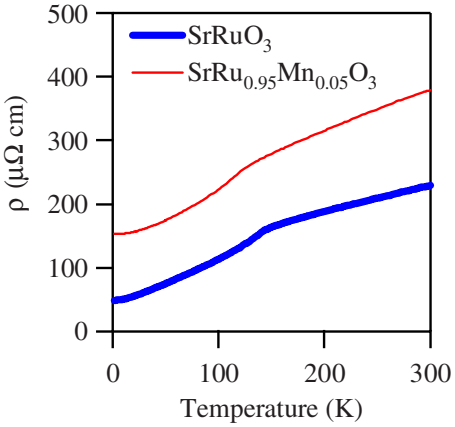

FIG. 1. (Color online) Temperature-dependent resistivity (ρ) of the $SrRuO_3$ (bold) and $SrRu_{0.95}Mn_{0.05}O_3$ (solid) thin films that were grown on $SrTiO_3(100)$ substrates. The increased resistivity and the reduced T_C are evident for the $SrRu_{0.95}Mn_{0.05}O_3$ thin film.

II. EXPERIMENT

Epitaxial thin film structures were fabricated by pulsed laser deposition using a KrF excimer laser with a fluence of 2.0 J/cm^2 on $SrTiO_3(100)$ substrates that are undoped and Nb=0.5 wt % doped in an oxygen partial pressure (P_{O2}) of 0.3 Torr (unless otherwise indicated), and at a substrate temperature of 800 °C. The deposited film thicknesses of $SrRuO_3$ and $SrRu_{0.95}Mn_{0.05}O_3$ were 800 Å. The polycrystalline $SrRu_{1-x}Mn_xO_3$ ($x=0,0.05,0.15$), $SrMnO_3$, $SrTi_{0.95}Mn_{0.05}O_3$, and single crystal $SrTiO_3$ targets were used.

The critical concentration required for the bulk metal-insulator transition in $SrRu_{1-x}Mn_xO_3$ is $x=0.4$ (Ref. 18). At $x=0.05$, predominantly studied here, $SrRu_{1-x}Mn_xO_3$ is reported to be a metal with a slightly increased resistivity and a reduced T_C. The x ray diffraction patterns of the thin films revealed high quality epitaxial growth and an out-of-plane lattice constant of 3.95 Å for both $SrRu_{0.95}Mn_{0.05}O_3$ and undoped $SrRuO_3$. As shown in Fig. 1, the temperature-dependent resistivity (ρ) of the films deposited on the insulating $SrTiO_3(100)$ substrates exhibited metallic behavior with a T_C and a residual resistivity of 150 K and 50 $\mu\Omega$ cm for $SrRuO_3$, and 140 K and 150 $\mu\Omega$ cm for $SrRu_{0.95}Mn_{0.05}O_3$.

III. RESULTS

A. Temperature-dependent *I-V* characteristics

The temperature-dependent *I-V* characteristics for $SrRuO_3/Nb:SrTiO_3$ and $SrRu_{0.95}Mn_{0.05}O_3/Nb:SrTiO_3$ are shown in Figs. 2(a) and 2(b), respectively. Ohmic contacts were made by Ag paste directly on the ruthenates and Al deposition on $Nb:SrTiO_3$. The polarity of the applied bias is defined as a positive voltage applied to the ruthenate.

In the case of the $SrRuO_3$ junction, the forward bias current in the semilogarithmic plot is linearly proportional to the bias voltage with an overall shift to higher voltages at lower temperatures, indicating a near ideal Schottky behavior. The

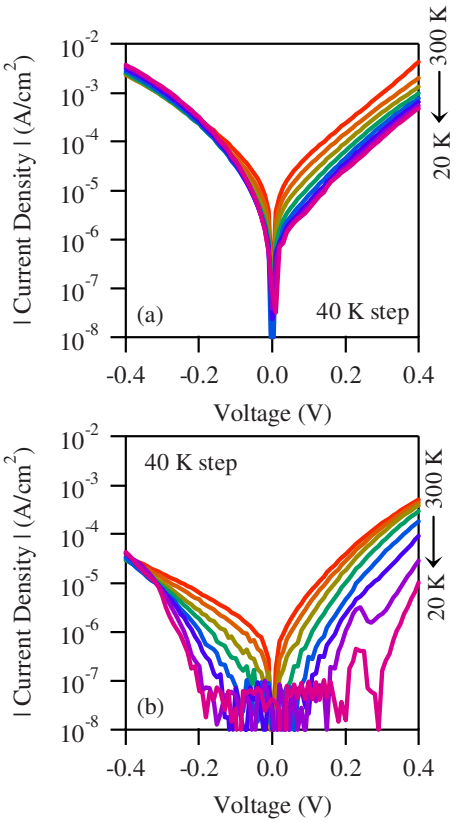

FIG. 2. (Color online) Temperature dependence of the *I-V* characteristics in the (a) $SrRuO_3/Nb:SrTiO_3$ and (b) $SrRu_{0.95}Mn_{0.05}O_3/Nb:SrTiO_3$ junctions. Measurements were taken between 300 and 20 K in 40 K steps.

current transport mechanism of these junctions was determined from the Richardson plot shown in Fig. 3(a). The reduced slope at high temperatures indicates the contribution of the thermoionic field emission, which is consistent with the large reverse bias current caused by the high doping concentration in $Nb:SrTiO_3$. The gradual increase in J_S/T^2 at low temperatures corresponds to the dominance of the field emission (FE) process in this temperature regime. Here, J_S is the saturation current density obtained by a linear extrapolation of the forward biased region of the *I-V* characteristics to zero voltage. The temperature dependence of the two junctions is very similar to what has been observed in $Au/Nb:SrTiO_3$ Schottky junctions.[11,19]

In contrast, two apparent differences can be seen in the *I-V* characteristics of the $SrRu_{0.95}Mn_{0.05}O_3/Nb:SrTiO_3$ junction compared to the $SrRuO_3/Nb:SrTiO_3$ junction (Fig. 2). First, the large decrease in the current over the measured voltage range by almost an order of magnitude, and second, the appearance of current peaks and negative differential resistance (NDR) at the forward bias below 60 K. Since the NDR behavior is observed in the FE low temperature region, the Mn substitution appears to induce a resonant state similar to a double barrier resonant tunneling diode.[20] A linear plot of the magnified *I-V* characteristics and the normalized conductance for $SrRu_{0.95}Mn_{0.05}O_3$ is shown in Figs. 4(a) and 4(b), respectively. As the temperature is decreased, a current peak emerges at $\sim+0.25$ V. The measurements taken under

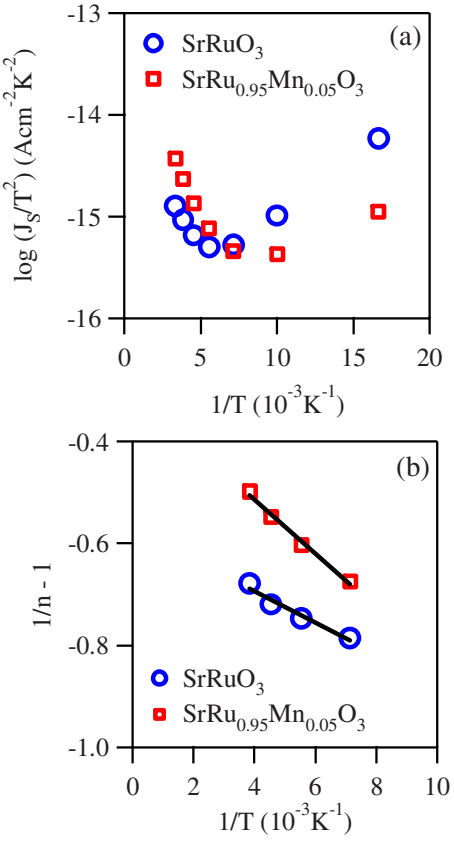

FIG. 3. (Color online) (a) Richardson plot of $SrRuO_3$ ($SrRu_{0.95}Mn_{0.05}O_3$)/Nb:$SrTiO_3$ junctions showing a crossover from the thermoionic field emission to the field emission. (b) Evaluation of the Schottky barrier height spatial inhomogeneity from the ideality factors. The circles (squares) denote $SrRuO_3$ ($SrRu_{0.95}Mn_{0.05}O_3$) and the lines are linear fits to the experimental data in the high temperature regime.

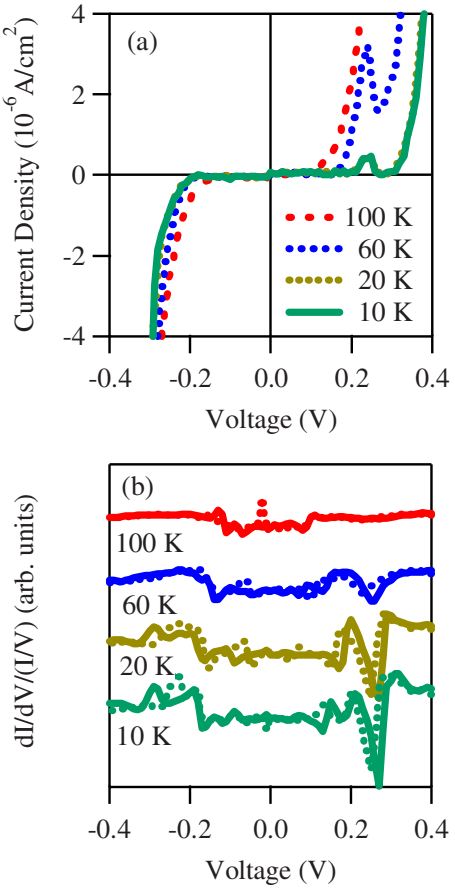

FIG. 4. (Color online) Temperature dependence of the (a) *I-V* characteristics and (b) the normalized conductance in a $SrRu_{0.95}Mn_{0.05}O_3$/$SrTiO_3$ junction. Solid (dotted) lines in (b) denote the voltage sweeps in the positive (negative) direction. The NDR emerges as the temperature is decreased.

an applied magnetic field of 13 T revealed no significant difference in either the peak voltage or the conductance, indicating that this is a charge state, not a collective magnetic state.

The large decrease in the current can be quantitatively addressed by analyzing the temperature dependence of the junction ideality factor, which indicates the degree of the spatial inhomogeneity of the Schottky barrier heights (Φ_{SB}).[21] The assumptions of a Gaussian distribution and voltage dependence of the Φ_{SB} give the following relationship, which agrees with many experimental results:[21]

$$\frac{1}{n(T)} - 1 = \rho_2 + \frac{\rho_3}{2kT/q}. \quad (1)$$

Here, n is the ideality factor, k the Boltzmann constant, and q the electronic charge. ρ_2 is a measure of the sensitivity of Φ_{SB} to the applied voltage and ρ_3 corresponds to the standard deviation in Φ_{SB}. The present results that were plotted following Eq. (1) are shown in Fig. 3(b). The obtained values, ρ_2 and ρ_3, are −0.57 and 5.31 meV for $SrRuO_3$, and −0.30 and 9.08 meV for $SrRu_{0.95}Mn_{0.05}O_3$. The increase in ρ_3 by almost a factor of two for the Mn-doped junction indicates that the presence of Mn ions increases the potential fluctuations at the interface.

B. Interface modulation

To verify the role of Mn doping on the NDR, we fabricated the modulated heterointerfaces where the Mn concentration was varied across the interface, as shown in Fig. 5(a). In the five structures, the location of the Mn ions is systematically varied with respect to the interface. Structures with single unit cell (uc) features were deposited while monitoring the reflection high-energy electron diffraction (RHEED) intensity. A two stage differential pumping setup enabled the RHEED observations at high pressure.

In structure (1), one unit cell of $SrMnO_3$ is deposited on the Nb:$SrTiO_3$ substrate at P_{O2}=0.1 Torr, followed by a thick layer of $SrRuO_3$. The reduced current density in the whole voltage range at 20 K can be attributed to the high resistivity of $SrMnO_3$ at low temperatures and, as is evident from Fig. 5(b), no NDR was observed. In structure (2). the surface of the Nb:$SrTiO_3$ is fully covered with $SrRu_{0.95}Mn_{0.05}O_3$, as discussed above. In structure (3), one unit cell of $SrRu_{0.95}Mn_{0.05}O_3$, grown at P_{O2}=0.1 Torr, is inserted between a thick layer of $SrRuO_3$ and the Nb:$SrTiO_3$

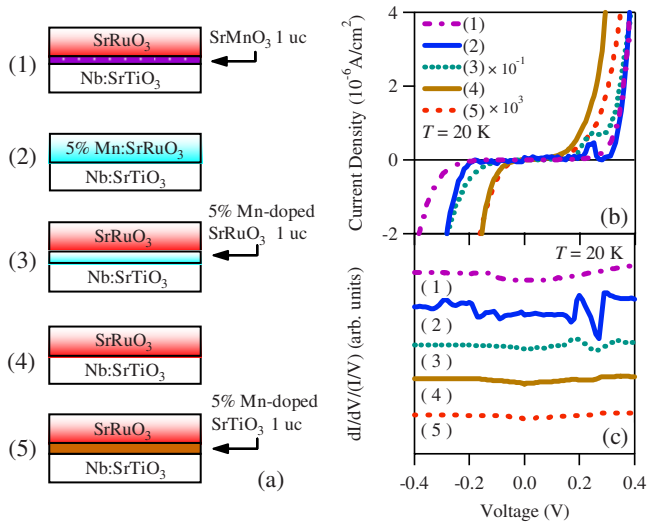

FIG. 5. (Color online) (a) Schematic diagram of the artificial structures grown to systematically vary the distribution of the Mn ions with respect to the interface. (1) $SrRuO_3/[SrMnO_3]_{1uc}/Nb:SrTiO_3$, (2) $SrRu_{0.95}Mn_{0.05}O_3/Nb:SrTiO_3$, (3) $SrRuO_3/[SrRu_{0.95}Mn_{0.05}O_3]_{1uc}/Nb:SrTiO_3$, (4) $SrRuO_3/Nb:SrTiO_3$, and (5) $SrRuO_3/[SrTi_{0.95}Mn_{0.05}O_3]_{1uc}/Nb:SrTiO_3$. (b) The *I-V* characteristics and (c) the normalized conductance of the structures illustrated in (a). The NDR is observed only in structures (2) and (3).

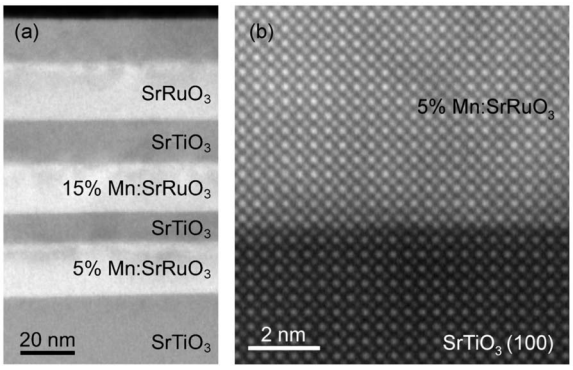

FIG. 6. Annular dark field STEM images of a $(SrRu_{1-x}Mn_xO_3/SrTiO_3)$ multilayer. (a) Overview of the structure. (b) High magnification image of the abrupt $SrRu_{0.95}Mn_{0.05}O_3/SrTiO_3$ interface.

substrate. The basic features of the *I-V* characteristics are the same as in $SrRuO_3/Nb:SrTiO_3$ but with the presence of a current peak, implying that the origin of the observed NDR is not caused by the modification of the band alignment but by the modification of the local interface structure. Structure (4) is the case of $SrRuO_3/Nb:SrTiO_3$, which is shown again for comparison. The extreme case, simulating a situation where the Mn ions are embedded inside $Nb/SrTiO_3$, is demonstrated in structure (5). Here, a single unit cell of $SrTi_{0.95}Mn_{0.05}O_3$ was deposited on $Nb:SrTiO_3$ at $P_{O2}=1.0\times10^{-5}$ Torr, followed by the deposition of $SrRuO_3$. From the investigations of the leakage current at metal/Mn-doped $SrTiO_3$ contacts, the Mn-doped $SrTiO_3$ is known to be insulating.[22,23] In this case also, no NDR was observed.

The above investigation has given evidence that the appearance of the low temperature NDR is associated with the presence of a low concentration of Mn ions on the metal side, ruling out the possibility of Mn, embedded in the substrate by diffusion or implantation, acting as ionic potentials within the depletion region.[24,25] The absence of the current peak in structure (1) is ascribed to the formation of a $SrMnO_3$ *band* rather than the isolated atomic states at the interface.

C. Electron microscopy and spectroscopy

The microscopic structure of the ruthenate/titanate interface was analyzed using scanning transmission electron microscopy (STEM) performed in a 200 kV FEI Tecnai F20 STEM. A superlattice of $SrRuO_3$ (20 nm)/$SrTiO_3$ (10 nm)/$SrRu_{0.85}Mn_{0.15}O_3$ (20 nm)/$SrTiO_3$ (10 nm)/$SrRu_{0.95}Mn_{0.05}O_3$ (20 nm) was fabricated on a $SrTiO_3(100)$ substrate [Fig. 6(a)]. An annular dark field STEM image of the interface between the substrate and the first ruthenate layer, $SrRu_{0.95}Mn_{0.05}O_3$, is shown in Fig. 6(b), demonstrating that the interface is chemically abrupt, with no obvious defects or dislocations. All Schottky junctions analyzed in this work were prepared under similar conditions, as shown in the test structure above, suggesting that the interfaces in these junctions are of comparable quality. In order to understand the local bonding of the Mn dopants in $SrRu_{1-x}Mn_xO_3$, electron energy loss spectroscopy was performed. From the simple picture of Mn for the Ru substitution in $SrRu_{0.95}Mn_{0.05}O_3$, a Mn valence state of 4+ is expected; however, Mn^{3+} can also be present due to a charge disproportionation in the form of $Mn^{4+}+Ru^{4+}\rightleftharpoons Mn^{3+}+Ru^{5+}$ (Ref. 26). In Fig. 7, the Mn-$L_{2,3}$ spectra for the three ruthenate layers are compared to the Mn^{3+} and Mn^{4+} reference spectra obtained from bulk $LaMnO_3$ and $SrMnO_3$,

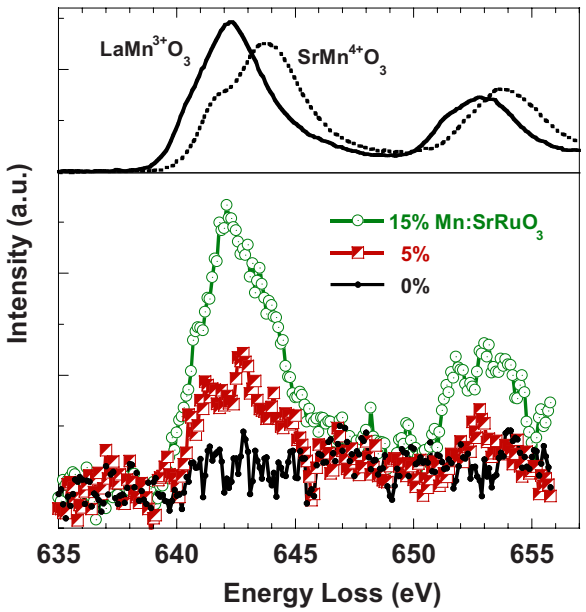

FIG. 7. (Color online) Mn-$L_{2,3}$ electron energy loss spectra from the three Mn-doped $SrRuO_3$ layers imaged in Fig. 6(a). For comparison, the Mn^{3+} and Mn^{4+} reference spectra are shown.

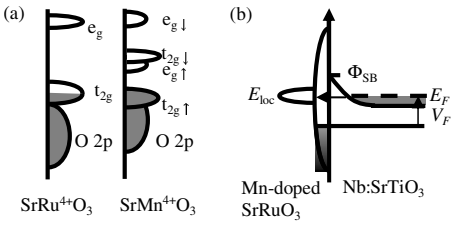

FIG. 8. (a) A schematic of the density of states for $SrRuO_3$ and $SrMnO_3$. (b) An interface band diagram illustrating the localized state on the metal side of the interface. V_F is the applied forward bias voltage, E_F is the Fermi level, Φ_{SB} the Schottky barrier height, and E_{loc} is the localized state at the interface.

respectively.[27] From the peak position of the Mn-L_3 edge, a Mn valence of 3 ± 0.3 in the Mn-doped ruthenate layers can be inferred.

IV. DISCUSSION

From the above studies, we have found that the impurity doping on the metal side can strongly influence the electronic structure at the interface. We consider the relation between the Mn doping in $SrRuO_3$ and the NDR by examining the electronic structures of the two parent compounds $SrRuO_3$ and $SrMnO_3$. In $SrRuO_3$, the crystal field splitting $10Dq$ of ~ 3 eV is obtained from optical spectroscopy measurements,[28] and the oxygen $2p$ band lies below the Ru t_{2g} band where the Fermi level is located, as shown in Fig. 8(a). We base our discussion on $SrMnO_3$ with a cubic G-type antiferromagnetic ground state, for which the theoretically calculated density of states are schematically shown in Fig. 8(a). The top of the valence band overlaps with the oxygen $2p$ band and the Mn e_g bands are located ~ 0.3 eV above the Fermi level.[29] Within a rigid band picture, the Ru to Mn substitution modifies the empty states of $SrRuO_3$ arising from the Mn e_g states. Furthermore, the doping independent lattice constant favors Mn ions to be localized owing to their smaller cation radius.

The observation of the current peak at the *forward* bias and below 1.47 eV, the Φ_{SB} of $SrRuO_3/Nb:SrTiO_3(100)$,[8] further support the above band structure consideration. Only when the localized states (E_{loc}) lie between the Fermi level (E_F) and Φ_{SB} can NDR be observed under the *forward* bias, as illustrated in Fig. 8(b). In other cases, either the current will be dominated by the large FE current or the localized states are buried in the large density of states of the host. We conclude that the NDR observed at the $SrRu_{0.95}Mn_{0.05}O_3/Nb:SrTiO_3$ interface is caused by the localized Mn e_g states inside $SrRu_{0.95}Mn_{0.05}O_3$ acting as the resonant state.

V. CONCLUSIONS

We have applied the highly sensitive response of metallic perovskites to the impurities in a Schottky junction to demonstrate that the interface electronic structure can be strongly modified by the introduction of substitutional impurities on the *metal* side. The change in the junction characteristics induced by impurity doping is unexpectedly large considering the small differences in the in-plane bulk transport properties. In addition to the enhanced spatial fluctuation of the interface potential, the dispersed Mn ions act as resonant states, giving rise to the NDR in the I-V characteristics. The poor electrostatic screening generally present in metallic perovskites and the close similarity in the chemical bonding between metallic and semiconducting perovskites can result in robust interface states exhibiting the character of the impurity element. Further studies may lead to designing the resonant tunneling structures by the simple doping of a metallic host or as a prototypical structure for spectroscopic investigation of screening, localization, and metal-insulator transitions in strongly correlated electron systems.

ACKNOWLEDGMENTS

This work was supported by the TEPCO Research Foundation and a Grant-in-Aid for Scientific Research on Priority Areas. Y.H. acknowledges support from the Grant-in-Aid 21st Century COE Program at the University of Tokyo. The work at Cornell University was supported under the ONR EMMA MURI monitored by Colin Wood. L.F.K. acknowledges financial support by Applied Materials.

*hikita@k.u-tokyo.ac.jp
†Present address: Materials and Structures Laboratory, Tokyo Institute of Technology, Yokohama, Kanagawa 226-8503, Japan.

[1] A. Beck, J. G. Bednorz, C. Gerber, C. Rossel, and D. Widmer, Appl. Phys. Lett. **77**, 139 (2000).
[2] N. Nakagawa, M. Asai, Y. Mukunoki, T. Susaki, and H. Y. Hwang, Appl. Phys. Lett. **86**, 082504 (2005).
[3] H. Katsu, H. Tanaka, and T. Kawai, Appl. Phys. Lett. **76**, 3245 (2000).
[4] E. H. Rhoderick and R. H. Williams, *Metal-Semiconductor Contacts* (Clarendon, Oxford, 1988).
[5] V. Heine, Phys. Rev. **138A**, 1689 (1965).
[6] M. Imada, A. Fujimori, and Y. Tokura, Rev. Mod. Phys. **70**, 1039 (1998).
[7] N. Nakagawa, H. Y. Hwang, and D. A. Muller, Nat. Mater. **5**, 204 (2006).
[8] Y. Hikita, Y. Kozuka, T. Susaki, H. Takagi, and H. Y. Hwang, Appl. Phys. Lett. **90**, 143507 (2007).
[9] M. Minohara, I. Ohkubo, H. Kumigashira, and M. Oshima, Appl. Phys. Lett. **90**, 132123 (2007).
[10] T. Yamamoto, S. Suzuki, K. Kawaguchi, and K. Takahashi, Jpn. J. Appl. Phys., Part 1 **37**, 4737 (1998).
[11] T. Susaki, Y. Kozuka, Y. Tateyama, and H. Y. Hwang, Phys. Rev. B **76**, 155110 (2007).
[12] P. B. Allen, H. Berger, O. Chauvet, L. Forro, T. Jarlborg, A. Junod, B. Revaz, and G. Santi, Phys. Rev. B **53**, 4393 (1996).

[13] L. Klein, J. S. Dodge, C. H. Ahn, G. J. Snyder, T. H. Geballe, M. R. Beasley, and A. Kapitulnik, Phys. Rev. Lett. **77**, 2774 (1996).
[14] F. Fukunaga and N. Tsuda, J. Phys. Soc. Jpn. **63**, 3798 (1994).
[15] L. Pi, A. Maignan, R. Retoux, and B. Raveau, J. Phys.: Condens. Matter **14**, 7391 (2002).
[16] C. Bansal, H. Kawanaka, R. Takahashi, and Y. Nishihara, J. Alloys Compd. **360**, 47 (2003).
[17] G. N. Banerjee, R. N. Bhowmik, and R. Ranganathan, J. Phys.: Condens. Matter **13**, 9481 (2001).
[18] G. Cao, S. Chikara, X. N. Lin, E. Elhami, V. Durairaj, and P. Schlottmann, Phys. Rev. B **71**, 035104 (2005).
[19] H. Hasegawa and T. Nishino, J. Appl. Phys. **69**, 1501 (1991).
[20] R. Tsu and L. Esaki, Appl. Phys. Lett. **22**, 562 (1973).
[21] J. H. Werner and H. H. Guttler, J. Appl. Phys. **69**, 1522 (1990).
[22] W. Hofman, S. Hoffmann, and R. Waser, Thin Solid Films **305**, 66 (1997).
[23] K. Morito, T. Suzuki, and M. Fujimoto, Jpn. J. Appl. Phys., Part 1 **40**, 5493 (2001).
[24] S. Modesti, D. Furlanetto, M. Piccin, S. Rubini, and A. Franciosi, Appl. Phys. Lett. **82**, 1932 (2003).
[25] J. Caro, I. D. Vink, G. D. J. Smit, S. Rogge, T. M. Klapwijk, R. Loo, and M. Caymax, Phys. Rev. B **69**, 125324 (2004).
[26] R. K. Sahu, Z. Hu, M. L. Rao, S. S. Manoharan, T. Schmidt, B. Richter, M. Knupfer, M. Golden, J. Fink, and C. M. Schneider, Phys. Rev. B **66**, 144415 (2002).
[27] $LaMnO_3$ bulk specimen was supplied by Toshima Manufacturing Co., Ltd. $SrMnO_3$ specimen was prepared by sintering $SrCO_3$ and MnO_2 in molar ratio at 1300 °C for 24 h repeatedly with interval grinding.
[28] Y. S. Lee, J. S. Lee, T. W. Noh, D. Y. Byun, K. S. Yoo, K. Yamaura, and E. Takayama-Muromachi, Phys. Rev. B **67**, 113101 (2003).
[29] R. Sondena, P. Ravindran, S. Stolen, T. Grande, and M. Hanfland, Phys. Rev. B **74**, 144102 (2006).